Engineering Fracture Mechanics 134 (2015) 304–316

Contents lists available at ScienceDirect

Engineering Fracture Mechanics

journal homepage: www.elsevier.com/locate/engfracmech

Evaluation of indentation fracture toughness for brittle materials based on the cohesive zone finite element method

Hong Chul Hyun [a], Felix Rickhey [a], Jin Haeng Lee [b,*], Minsoo Kim [a], Hyungyil Lee [a]

[a] Dept. of Mechanical Engineering, Sogang University, Seoul 121-742, Republic of Korea
[b] Research Reactor Mechanical Structure Design Division, Korea Atomic Energy Research Institute, Daejeon 305-353, Republic of Korea

ARTICLE INFO

Article history:
Received 28 April 2014
Received in revised form 26 November 2014
Accepted 27 November 2014
Available online 5 December 2014

Keywords:
Fracture toughness
Indentation cracking
Cohesive zone model
Indenter geometry
Vickers indentation
Berkovich indentation
Nanoindentation

ABSTRACT

We propose indentation fracture toughness evaluation methods based on finite element analysis adapting the cohesive zone model. Establishing an appropriate finite element model, we examine the effects of material properties on the size of the cracks formed by Vickers indentation, and then suggest a regression formula for the estimation of the fracture toughness. The formula is extended to other types of pyramidal indenters including variations of the indenter angle and the number of indenter edges. The suggested methods are examined by comparison of the experimental data, and the fracture toughness can be accurately estimated from pyramidal indentation data.

1. Introduction

In contrast to conventional fracture toughness evaluation methods, which require tedious preparation of the test specimens, the indentation test-based method does not require this kind of special specimen; instead, it can be directly applied to a part/structure with simple treatment of the surface. This huge advantage has led to numerous studies on evaluating the critical load corresponding to crack initiation or certain crack characteristics for Vickers, Berkovich, cube-corner, and other types of indenters. For brittle materials such as glass or ceramics, not only elastic–plastic deformation occurs during indentation due to stress concentrations beneath the indenter, but also various cracks can form around the impression. When using three- or four-sided pyramidal indenters, radial, median, semi-circular (half-penny) or lateral cracks can form independently and merge, depending on the material properties, the indenter geometry, and the indentation load. Based on these observations, numerous studies have been conducted to predict the fracture toughnesses of brittle materials from crack size, indentation load and/or other parameters [12,5,13,14,1,2,3,16,17,24,10,4,21,8]. The final goal of these studies is to find the fracture toughness similar to that obtained by conventional testing methods. However, indentation fracture toughnesses predicted by these formulas often exhibit quite a significant deviation from the fracture toughnesses of conventional methods, and therefore doubt remains regarding the reliability of the indentation cracking-based methods.

Before the 1950s, the cracks formed by indentation on brittle materials (to obtain hardness) were regarded as a disturbing phenomenon. Palmqvist [20] was the first performer who related the indentation crack length to the fracture toughness. He

* Corresponding author. Tel.: +82 42 868 4525; fax: +82 42 868 8622.
E-mail address: jinhaeng@kaeri.re.kr (J.H. Lee).

http://dx.doi.org/10.1016/j.engfracmech.2014.11.013
0013-7944/

Nomenclature

a	impression half-diagonal
c	crack length
E	Young's modulus
H	hardness
h	indentation depth
K_c	fracture toughness
l	crack length
P	indentation load
α	correction factor
δ_c	crack-initiating separation
δ_{max}	damage-initiating separation
ε_o	yield strain
Γ	fracture energy
κ	correction factor
ν	Poisson's ratio
σ_o	yield strength
σ_{max}	damage-initiating stress
ψ	centerline-to-face angle

showed that the average length of the cracks emanating from the corners of the impression can be used to infer the fracture toughness. Later, Lawn et al. [14] and Anstis et al. [1] applied Hill [6] and established a formula for calculating the fracture toughness from the crack length, the maximum indentation load, the hardness and the Young's modulus. Lawn et al. [14] findings are based on the following two experimental observations: first, the deformation under the indenter satisfies geometrical self-similarity; second, for "well-developed" cracks, the indentation load P is proportional to $c^{3/2}$ where c is the crack length (Fig. 1). The full equation includes the Young's modulus E, the hardness H and the indenter angle ψ as follows:

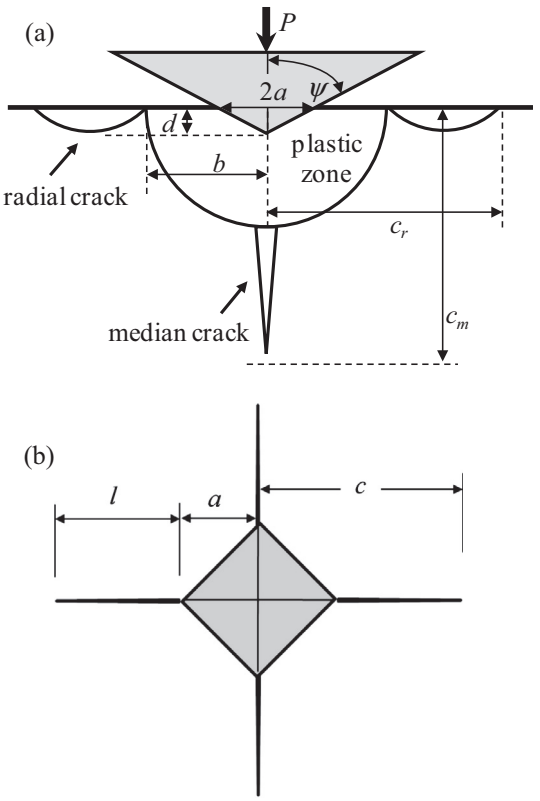

Fig. 1. Schematic of (a) the median and radial crack system and (b) the top view of Vickers indentation cracking geometry.

$$K_c \propto (a/b)(E/H)\cot\psi\frac{P}{c^{3/2}} \tag{1}$$

where a and b are the impression half-diagonal and the plastic zone size, respectively, as shown in Fig. 1. The ratio a/b is related to β_H (=b/r where r is the cavity radius) used in Hill's expanding cavity model, and β_H can be related to E/H. Based on Hill's expanding cavity model, H/E can be expressed as a function of b/r,

$$\frac{H}{E} = \frac{2[1+\ln(b/r)^3]}{9[(1-\nu)(b/r)^3 - 2(1-2\nu)/3]} \tag{2}$$

Lawn et al. [14] simply set $b/r \approx (E/H)^m$ and $m = 1/2$ from the regression of experimental results. Assuming that the cavity volume is equal to the volume of the impression generated by the pyramidal indenter, we can write

$$b/a \approx (E/H)^{1/2}(\cot\psi)^{1/3}. \tag{3}$$

since r is proportional to $a(\cot\psi/\pi)^{1/3}$. Combining Eqs. (1) and (3) yields the following expression for the fracture toughness K_c.

$$K_c = \alpha\left(\frac{E}{H}\right)^{1/2}\left(\frac{P}{c^{3/2}}\right). \tag{4}$$

Anstis et al. [1] calibration constant α is 0.016 ± 0.004 from Vickers indentation tests on glasses and ceramics. However, in contrast to Lawn et al. [14] and Anstis et al. [1], Laugier [10] used $b/r \approx (E/H)^m$ with $m = 1/3$; the exponent in Eq. (4) then becomes 2/3 and $\alpha = 0.0098 \pm 0.0025$. Eq. (4) based on Eq. (1) and Hill's expanding cavity model contains several assumptions and simplifications. Moreover, the coefficients m and α were not determined by physical bases, but determined by fitting of the experimental results with restrictedly chosen materials. In each of these studies, the deviation of α obtained from experimental data is about 25% although the inaccuracies in the fracture toughnesses are not merely due to α but may also come from inaccurately determined material properties. In addition, Jang and Pharr [8] expressed α as a function of indenter angle and Poisson's ratio, but Lee et al. [15] showed that α does not only depend on Poisson's ratio but is also influenced by other material properties. Therefore, for the accurate fracture toughness evaluation, the variations of α and crack morphology with respect to indenter shapes and material properties need to be thoroughly investigated. Meanwhile, Niihara et al. [16] suggested a method that distinguishes between radial ($c/a \leqslant 2.5$) and half-penny ($c/a \geqslant 2.5$) cracks, by using two kinds of crack lengths, l and c, as shown in Fig. 1,

$$\left(\frac{K_c\phi}{H_V a^{1/2}}\right)\left(\frac{H_V}{E\phi}\right)^{2/5} = 0.035(l/a)^{-1/2}; \quad (c/a \leqslant 2.5) \tag{5}$$

$$\left(\frac{K_c\phi}{H_V a^{1/2}}\right)\left(\frac{H_V}{E\phi}\right)^{2/5} = 0.129(c/a)^{-3/2}; \quad (c/a \geqslant 2.5) \tag{6}$$

where l is the crack length from a to the end of crack ($c = l + a$), $\phi(\approx 3)$ is constrain factor, and $H_V = 0.9272H$. However, it is difficult to infer the final crack shape based on the surface cracks only because radial and median cracks can be independently initiated and propagated during loading and/or unloading, and the critical c/a value of Niihara et al. [16] is also dependent on material properties and indenter shapes. Apart from the equations above, more than 30 other forms for determining the fracture toughness by indentation tests have been proposed. Ponton and Rawlings [22,23] assessed a number of such equations and found that there is a deviation of approximately 30% from the fracture toughnesses obtained by other conventional methods.

Recently, finite element analysis (FEA) approaches and various measuring techniques for diverse indenter shapes have been applied to accurately evaluate the fracture toughness considering the effects of material characteristics [27,25,15,9]. In particular, the cohesive interface model can be efficiently applied to the FE simulation of various crack problems [26,28,15,9,7]. Lee et al. [15] have performed FE indentation cracking analysis using the cohesive zone model (CZM) to analyze the influence of the four-sided indenter angle and material properties on the crack characteristics. Johanns et al. [9] have shown that the cohesive FE model can be used to examine the relationships between crack morphology, material properties, indenter geometry, and indentation test measurements from a two-dimensional standard CT specimen, a two-dimensional wedge, and three-dimensional Vickers and Berkovich indentation cracking analyses when the crack length is long enough in comparison to the cohesive zone size. Hyun et al. [7] have extended Lee et al. [15] approach and investigated the relation between the crack length and the number of indenter edges from the CZM-based FEA and experimental comparison. With the CZM, we can simulate the fracture process in material by using the fracture energy function.

In this study, based on the model proposed by Lee et al. [15], we establish new equations to determine the fracture toughness through the quantitative evaluation of the crack size obtained by FEA with respect to material properties (the Young's modulus, the yield strength, the Poisson's ratio, and the fracture toughness) and indentation conditions (the maximum indentation load, the number of indenter edges, and the indenter angle), and then verify the equations by comparing estimated fracture toughnesses with experimental results.

The paper is organized as follows. In Section 2, the finite element analysis procedures adapting cohesive zone model are introduced. In Section 3, preliminary FE analysis is performed to find the parameters that mainly influence the fracture toughness, and their influence on the crack length is analyzed. Based on the FE parametric study of Vickers indentation, we suggest mapping functions that express the fracture toughness in terms of the maximum indentation load, the crack

length, and material properties. We study then the influence of the number of indenter edges and the angle on the crack length, and extend the applicability of the proposed equation. In Section 4, the proposed fracture toughness equations are verified by comparison to indentation test data.

2. Cohesive zone finite element model

Lawn et al. [14] assumed α in Eq. (4) to be only dependent on the centerline-to-face angle ψ; but as shown by Lee et al. [15], it can vary with material properties and other indentation parameters. To study the effects of material properties and indenter geometry on the fracture toughness evaluation, the commercial package, ABAQUS/Standard, is used for the cohesive zone finite element simulations. The three-dimensional FE models for four-sided and three-sided pyramidal indentation simulations are generated as shown in Fig. 2. Because of the symmetric boundary conditions, an 1/4 model for four-sided indenters and an 1/3 model for three-sided indenters are used. For the simplicity of input material properties, elastic-perfectly plastic materials are assumed. The elastic diamond indenter with the Young's modulus $E_I = 1016$ GPa and the Poisson's ratio $\nu_I = 0.07$ is pressed into the top surface of the specimen while the bottom surface of it is fixed.

We put the cohesive elements where the crack can be initiated and propagated. In Johanns et al. [9] and Hyun et al. [7] observation, the cracks are generated along the indenter edges only irrespective of three-sided or four-sided indenter if the symmetric conditions are maintained, so the cohesive elements are located along the plane that is perpendicular to the material free surface and aligned with the edges of the indenter, as shown in Fig. 2.

The effects of the cohesive zone properties on the crack evolution and propagation are described and discussed by Lee et al. [15] and Johanns [9]. Although the phenomenological CZM has inherent limitation for relatively short cracks in comparison to the process zone size, the variation of the traction-separation properties has a negligible effect on the indentation cracking analysis for well-developed cracks when the fracture energy and other material properties are identical. In this study, we are interested in well-developed cracks, so we simply use the bilinear traction-separation model as shown in Fig. 3. The cohesive traction increases up to a critical (damage-initiating) separation ($\delta_{\max}$) between the cohesive interface, and decreases monotonically to zero upon further loading once the critical separation is exceeded. The area under the traction–separation curve in Fig. 3 represents the fracture energy Γ, so the fracture toughness can be inferred by

$$\Gamma = \frac{K_c^2}{E'} = \frac{1}{2}\sigma_{\max}\delta_c,\ E' = \begin{cases} E & : \text{ plane stress} \\ E/(1-\nu^2) & : \text{ plane strain} \end{cases} \tag{7}$$

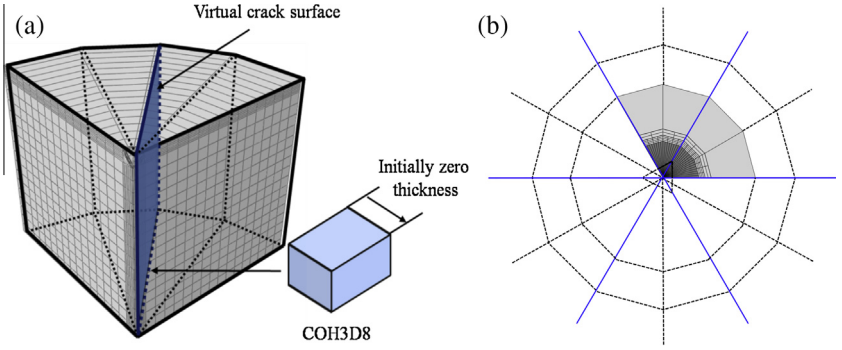

Fig. 2. (a) 1/4 FE model for four-sided and (b) 1/3 FE model for three-sided pyramidal indentation using cohesive zone model.

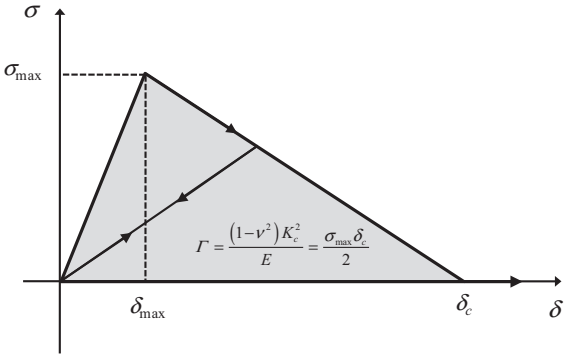

Fig. 3. The traction–separation relation for a bilinear cohesive zone model [15].

where v and E are the Poisson's ratio and the elastic (Young's) modulus; σ_{max}, δ_{max} and δ_c are the damage-initiating stress, the corresponding separation and the crack-initiating separation, respectively, as shown in Fig. 3. The plane strain relation is used to calculate the fracture energy. It should be noted that the purpose of the indentation cracking approach to the evaluation of fracture toughness is basically to get the mode I fracture toughness value. Theoretically, the radial/median/half-penny cracks are assumed to be developed in the symmetric plane only. The mode I stress intensity factor for the center-loaded half-penny crack is can be written by $K = 2aP/(pc)^{3/2}$ which is the fundamental form of the indentation fracture toughness evaluation where K is the mode I stress intensity factor [14]. The mode-II and mode-III type cracks cannot be considered irrespective of the number of cracks [19].

Both of the 1/4 model (for four-sided indenters) and the 1/3 model (for three-sided indenters) consist of approximately 86,600 elements and 97,000 nodes. For the three-sided indenter, the crack is not developed on the face plane, but developed on the edge plane only when the symmetric conditions are assumed in FEA, so we do not consider the crack development on the face plane, and the 1/3 model is used in the present work [7].

The detailed procedure to measure the crack length in FEA is also described in Lee et al. [15] and Hyun et al. [7] papers. The crack length depends on the definition of the crack front around the process zone in FEA, but the sensitivity to the definition decreases with the process zone size. In this study, we are interested in well-developed cracks, so the definition is not a critical factor. We simply assume that the crack forms when the cohesive traction has become zero, i.e., $\delta = \delta_c$. The damage-initiating stress is chosen as $\sim 0.1\sigma_o \leq \sigma_{max} \leq \sim 0.2\sigma_o$ (σ_o: yield strength) to ensure the crack generation and to satisfy the linear elastic fracture condition, i.e., $c \gg$ process zone size [15].

The contact area depends on the friction coefficient between the indenter and the specimen, and as a consequence, the stress state in the material varies with the friction coefficient, which again influences the crack size. As the Coulomb friction coefficient f increases, the crack length very slightly increases in FE analysis; however, when $f \geqslant 0.2$, the crack length does not increase further. The friction coefficient between the diamond and other materials is about 0.1, so f is assumed to be 0.1.

3. Evaluation of indentation fracture toughness based on FEA

3.1. Preliminary FE analysis for fracture toughness evaluation

Preliminary FE analysis is performed to set up indentation parameters for fracture toughness evaluation. We set the damage-initiating stress and the fracture energy as $\sigma_{max} = 0.5$ GPa and $\Gamma = 0.0025$ GPa μm, respectively, based on Lee et al. [15] work. When the fracture toughness, the yield strain ($\varepsilon_o \equiv \sigma_o/E$), the Poisson's ratio, and the indenter centerline-to-face angle are changed, we investigate the variation of the coefficient of Eq. (4), α.

When the Young's moduli (E) are 100, 200, 400 GPa and the Poisson's ratio is fixed as 0.3, the fracture toughness (K_c) values become 0.52, 0.74, 1.05 MPa $m^{1/2}$, respectively. Table 1 shows the effects of the fracture toughness and the yield strain on the coefficient α. Other parameters used in the simulation are also listed in Table 1. For fixed ε_o and Γ, α decreases with increasing E, and for fixed E and Γ, α decreases with increasing ε_o (i.e., σ_o). This means not only ε_o but also E itself has an influence on α. Table 2 shows when other material properties and parameters are fixed, α decreases with increasing the Poisson's ratio v. As mentioned by Lee et al. [15], the crack morphology is significantly dependent on the Poisson's ratio. Hence, the Poisson's ratio is another important parameter to accurately evaluate the fracture toughness whereas the value is simply

Table 1
The variations of c/a and α with respect to material properties K_c and ε_o for Vickers indentation.

$v = 0.3$, $\Gamma = 0.0025$ GPa μm
$h_{max} = 0.6$ μm, $\sigma_{max} = 0.5$ GPa, $\delta_{max}/\delta_c = 1/4$

K_c (MPa $m^{1/2}$)	ε_o (σ_o/E)	P_{max} (mN)	H (GPa)	c/a	α
0.52	0.025 (2.5/100)	42.6	5.7	1.58	0.0157
0.74	0.025 (5.0/200)	84.8	11.3	1.92	0.0149
1.05	0.025 (10/400)	168.8	22.5	2.23	0.0132
0.52	0.050 (5.0/100)	55.0	8.2	1.53	0.0127
0.74	0.050 (10/200)	113.9	17.0	1.83	0.0116
1.05	0.050 (20/400)	227.4	34.0	2.11	0.0102

Table 2
The variations of c/a and α with respect to Poisson's ratio for Vickers indentation.

$E = 200$ GPa, $\sigma_o = 5$ GPa, $\Gamma = 0.0025$ GPa μm
$h_{max} = 0.6$ μm, $\sigma_{max} = 0.5$ GPa, $\delta_{max}/\delta_c = 1/4$

K_c (MPa $m^{1/2}$)	v	P_{max} (mN)	H (GPa)	c/a	α
0.71	0.1	76.3	10.2	2.25	0.0191
0.72	0.2	80.1	10.7	2.10	0.0170
0.74	0.3	84.8	11.3	1.93	0.0150

Table 3
The variations of c/a and α with respect to Vickers indenter angle.

E = 200 GPa, ν = 0.3, σ_o = 5 GPa, K_c = 0.74 MPa m$^{1/2}$ (Γ = 0.0025 GPa μm) h_{max} = 1.0 μm, σ_{max} = 0.5 GPa, δ_{max}/δ_c = 1/4				
ψ (°)	P_{max} (mN)	H (GPa)	c/a	α
55	99.2	11.8	2.72	0.0217
68	231.7	10.6	2.45	0.0159
75	426.1	10.3	2.17	0.0107

assumed to be 0.25 in the LEM form, Eq. (4). Table 3 shows the variation of α with respect to the centerline-to-face angle ψ. As the indenter angle increases, α decreases. This is because at the same maximum indentation loads, lower ψ results in a larger indent volume, which produces longer cracks and a larger α.

Consequently, for the accurate evaluation of the fracture toughness, the evaluation formulas should be set up to take into account the effects of the yield strain ε_o, the Young's modulus E, the Poisson's ratio ν, and indenter angle ψ.

3.2. Fracture toughness evaluation forms based on a parametric study

In Section 3.1, we have shown that α in Eq. (4) is a function of ε_o, E, ν and ψ. However, the hardness in Eq. (4) is not a material property because it can vary with indenter geometry, so it is a function of other material properties. In the present work, we preferentially reform the evaluation formula excluding the hardness. Based on the relationship between the maximum indentation load and the crack length for the well-developed crack system, i.e., $P_{max} \propto c^{3/2}$ [11], we can express the fracture toughness as a function of cot ψ, ν, ε_o, and E as follows:

$$\frac{K_c}{P_{max}/c^{3/2}} = \kappa(\cot\psi, \nu, \varepsilon_o, E). \tag{8}$$

In this section, we investigate the effect of each parameter on the coefficient κ, and then establish a new relation to evaluate the fracture toughness based on the FE parametric study. Afterwards, we suggest another equation to relate the material properties to the hardness.

FE analyses for four-sided pyramidal indentation are performed for each combination of five yield strains (ε_o = 0.02, 0.04, 0.06, 0.08, 0.1), four Poisson's ratios (ν = 0.1, 0.2, 0.3, 0.4), two centerline-to-face angles (ψ = 55°, 68°), and four Young's moduli (E = 100, 200, 400, 600 GPa). Jang and Pharr [8] experimental and Hyun et al. [7] FE results confirmed that the crack length c is proportional to $(\cot\psi)^{4/9}$, so the coefficient κ in Eq. (8) is proportional to $(\cot\psi)^{2/3}$. We therefore first establish an equation to predict fracture toughness for Vickers indenters (ψ = 68°), and then the equation is extended to other types of indenters by using $\kappa \propto (\cot\psi)^{2/3}$. We set Γ = 0.0025, 0.0010 GPa μm and E = 100, 200, 400, 600 GPa, so the fracture toughness becomes around 0.5–2 MPa μm$^{1/2}$, which depends on the Poisson's ratio. The materials are indented until the cracks are well-developed, and κ values are then evaluated. For each E, we observe the influences of ε_o and ν on κ_V where κ_V is the κ obtained with Vickers indentation (centerline-to-face angle ψ = 68°). Fig. 4 shows κ_V–ε_o relation with respect to the Poisson's ratio for E = 400 GPa. When Γ, E and ε_o are fixed, κ_V decreases with increasing ν. This can be explained by the fact that the decrease in ν makes cracks further developed during the unloading as described by Lee et al. [15], and because the load deviation caused by the change of the Poisson's ratio is relatively small, $P_{max}/c^{3/2}$ increases with ν which makes κ_V decreased. When Γ, E and ν are fixed, κ_V decreases with increasing ε_o, which means the increase in the yield resistance results in shorter cracks.

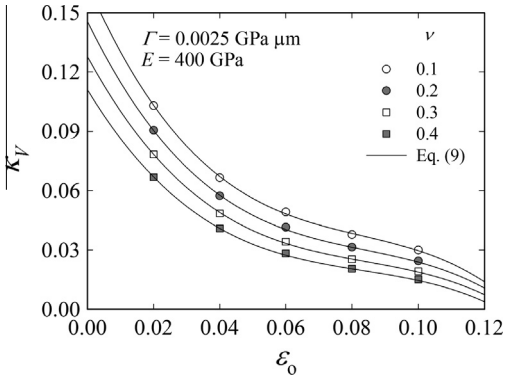

Fig. 4. κ_V vs. ε_o with respect to Poisson's ratio for Vickers indentation (Γ = 0.0025 GPa μm, E = 400 GPa). The regression lines obtained from Eq. (9) are also plotted.

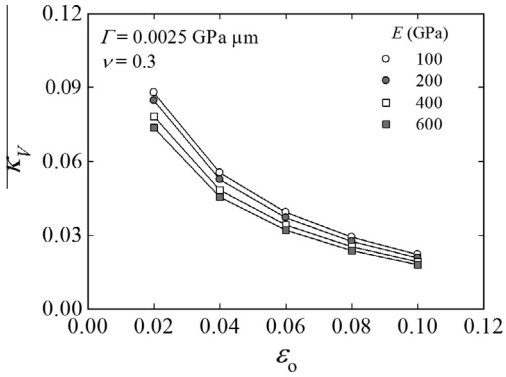

Fig. 5. κ_V vs. ε_o with respect to Young's modulus for Vickers indentation (Γ = 0.0025 GPa μm, ν = 0.3).

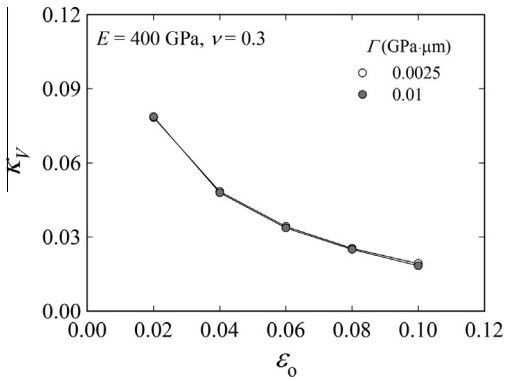

Fig. 6. κ_V vs. ε_o with respect to fracture toughness for Vickers indentation (E = 400 GPa, ν = 0.3).

When the material properties are fixed as Γ = 0.0025 GPa μm and ν = 0.3, the variations of κ_V with respect to E and ε_o are examined. As shown in Fig. 5, when ε_o is fixed, κ_V decreases with increasing E, which is the same as the results from the LEM form in Section 3.1. Fig. 6 shows the effect of the Γ (or K_c) on κ_V. When E = 400 GPa and ν = 0.3, κ_V values are obtained for the five yield strains. The κ_V values obtained with Γ = 0.010 GPa μm (K_c = 2.0966 MPa m$^{1/2}$) are good agreement with them with Γ = 0.0025 GPa μm (K_c = 1.0482 MPa m$^{1/2}$). Thus, when E, ν and ε_o are fixed, κ_V values are independent of Γ (or K_c), which means Eq. (8) is a reasonable form. To consider the influence of E on κ_V, we use E_R, the ratio of E to a reference Young's modulus, 1000 GPa ($E_R = E/E_{1000}$), which is similar to the indenter modulus, for the normalization of E.

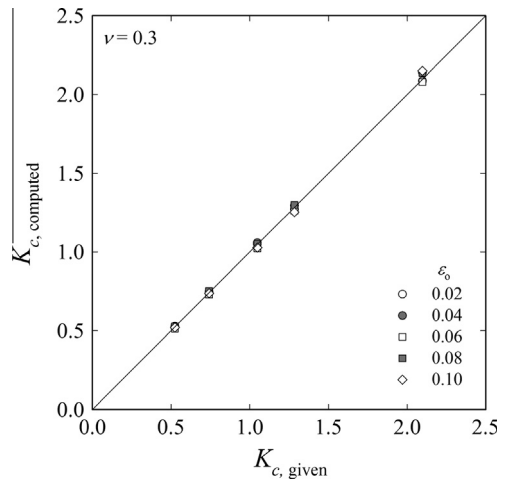

Fig. 7. The comparison of the fracture toughnesses computed from Eq. (9) to those imposed on FE model.

3.3. Regression analyses

The following procedure is used for the regression of each variable. First, for a given yield strain and Poisson's ratio, we regress to E_R. The obtained regression coefficients are regressed to the yield strain, and finally to the Poisson's ratio. Eq. (9) is a unified equation that takes into account each variable, *i.e.*, the Young's modulus ratio, the yield strain and the Poisson's ratio.

$$\begin{aligned} &K_c = \kappa_V(\nu, \varepsilon_o, E_R) P_{max}/c^{3/2} \\ &\kappa_V(\nu, \varepsilon_o, E_R) = \alpha_i^{\kappa}(\nu, \varepsilon_o)(E_R)^i; \quad i = 0,1,2 \\ &\alpha_i^{\kappa}(\nu, \varepsilon_o) = \beta_{ij}^{\kappa}(\nu)\varepsilon_o^j; \quad j = 0,1,2,3 \\ &\beta_{ij}^{\kappa}(\nu) = \gamma_{ijk}^{\kappa}\nu^k; \quad k = 0,1,2 \end{aligned} \tag{9}$$

where we use the Einstein summation convention, and α_i, β_{ij}, and γ_{ijk} are coefficients of the polynomial. The values of coefficients are given in Appendix A. The regression lines for Γ = 0.0025 GPa μm and E = 400 GPa are depicted in Fig. 4, and the input values of FEA and predicted fracture toughnesses are plotted in Fig. 7. The average deviation between calculated K_c values and those given is 1.2%.

As described before, κ is linear to $(\cot\psi)^{2/3}$. Hence, for example, the relationship between the κ values obtained with the ψ = 55° four-sided indenter and the ψ = 68° Vickers indenter can be derived:

$$\kappa_{4-55^\circ} = \kappa_V \left(\frac{\cot 55^\circ}{\cot 68^\circ}\right)^{2/3}. \tag{10}$$

where the subscript 4–55° means the 55° four-sided indenter. Hence, Eq. (9) based on Vickers indentation becomes

$$K_c = \kappa_V(\nu, \varepsilon_o, E_R)\left(\frac{\cot 55^o}{\cot 68^\circ}\right)^{2/3} P_{max}/c^{3/2}. \tag{11}$$

By using the maximum load and the crack length obtained from FE simulation with ψ = 55° four-sided pyramidal indenter, the fracture toughnesses are calculated as listed in Table 4. The average and the maximum deviations between input and predicted fracture toughnesses are about 2% and 4%, respectively.

Another factor related to the indenter geometries is the number of the edges (cracks), n_c. Hyun et al. [7] have suggested the following equation,

$$c_{Vn_c}/c_V = k_1 e^{-k_2 n_c}; (k_1, k_2) = (1.3680, 0.0778), \quad n_c \geqslant 3 \ (n_c \text{ is an integer}) \tag{12}$$

where c_V is the crack length obtained from Vickers indentation, and c_{Vn_c} is the crack length that can be obtained from another pyramidal indenter having n_c edges when their ideal contact areas (without consideration of the pile-up/sink-in effect) are equivalent. For example, n_c = 3 means the Berkovich indenter. When applying the relation between the crack size and the number of cracks at the same indentation load, we obtain the following fracture toughness equation for Berkovich indentation;

$$K_c = \kappa_B(\nu, \varepsilon_o, E_R) P_{max}/c_B^{3/2} = \kappa_V(\nu, \varepsilon_o, E_R)\left(k_1 e^{-3k_2}\right)^{3/2} P_{max}/c_B^{3/2} \quad k_1, k_2 = 1.3680, 0.0778 \tag{13}$$

where the subscript B means a Berkovich indenter. If an n_c-sided indenter with arbitrary centerline-to-face angle ψ is used, Eq. (13) can be further revised as follows:

$$K_c = \kappa_{n_c}(\nu, \varepsilon_o, E_R) P_{max}/c_{n_c}^{3/2} = \kappa_V(\nu, \varepsilon_o, E_R)\left(k_1 e^{-n_c k_2}\right)^{3/2}\left(\frac{\cot\psi_{n_c}}{\cot\psi_{Vn_c}}\right)^{2/3} P_{max}/c_{n_c}^{3/2} \quad k_1, k_2 = 1.3680, 0.0778 \tag{14}$$

where subscript n_c means an n_c-sided indenter, and Vn_c means an n_c-sided indenter equivalent to the Vickers indenter.

Table 4
The comparison of the fracture toughnesses obtained from Eq. (11) to those given for ψ = 55° four-sided pyramidal indentation.

ν = 0.3, ε_o = 0.04, Γ = 0.0025 GPa μm, σ_{max} = 0.5 GPa, δ_{max}/δ_c = 1/4					
Given K_c (MPa m$^{1/2}$)	h_{max}	E (GPa)	κ_{4-55°	Computed K_c (MPa m$^{1/2}$)	Error (%)
0.5241	1.5	100	0.0831	0.5148	1.8
0.7412		200	0.0780	0.7297	1.6
1.0483		400	0.0718	1.030	1.8
1.2839		600	0.0691	1.233	4.0
2.0966[a]	5.0	400	0.0712	2.077	0.94

[a] Γ = 0.010 GPa μm.

Table 5
The comparison of fracture toughnesses obtained from Eq. (13) to those given for Berkovich indentation.

$\nu = 0.3$, $\varepsilon_o = 0.04$, $\Gamma = 0.0025$ GPa·μm, $\sigma_{max} = 0.5$ GPa, $\delta_{max}/\delta_c = 1/4$					
Given K_c (MPa m$^{1/2}$)	h_{max}	E (GPa)	κ_B	Computed K_c (MPa m$^{1/2}$)	Error (%)
0.5241	1.5	100	0.0657	0.5028	4.1
0.7412		200	0.0614	0.7242	2.3
1.0483		400	0.0575	1.005	4.1
1.2839		600	0.0542	1.226	4.5

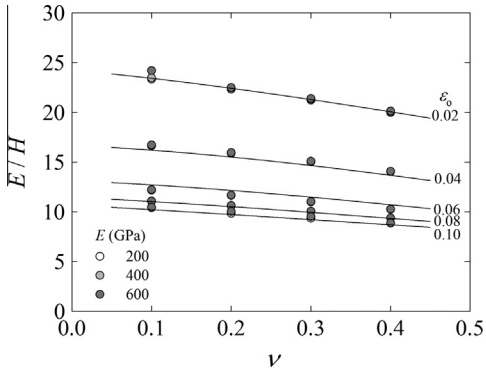

Fig. 8. E/H vs. ν for five yield strains. The effect of Young's modulus variation is negligible. The regression lines obtained from Eq. (15) are also plotted.

The maximum load and the crack length are acquired from the Berkovich indentation simulations, which are substituted into Eq. (13) to predict the fracture toughness. As shown in Table 5, the maximum deviation between input and calculated fracture toughnesses is below 5%.

Eqs. (9), (13) and (14) use the yield strain ε_o as an input parameter, but it is an additional parameter that cannot be directly obtained from the indentation test. We therefore replace the regression parameter ε_o by E/H for Vickers indentation, thereby making the evaluation method more practical. The relation between E/H, the Poisson's ratio and the yield strain is observed by FE analysis. From Fig. 8, it can be seen that E/H decreases with increasing ν and ε_o, and when ε_o is fixed, E/H is almost constant irrespective of E. For four Poisson's ratios and five yield strains, we establish a relation between material properties and E/H using a regression method similar to previous equations. The regression formula becomes

$$\begin{aligned} E/H &= f_0(\nu) + f_1(\nu) e^{-f_2(\nu)\varepsilon_o} \\ f_i(\nu) &= g_{ij}\nu^j; \quad i,j = 0,1,2 \end{aligned} \tag{15}$$

where we use the Einstein summation convention, and g_{ij} is a coefficient of the polynomial. The values of coefficients are given in Appendix A. Eq. (15) can be reversely written as follows:

$$\begin{aligned} \varepsilon_o &= -\frac{1}{f_2(\nu)} \ln\left(\frac{E/H - f_0(\nu)}{f_1(\nu)}\right) \\ f_i(\nu) &= g_{ij}\nu^j; \quad i,j = 0,1,2. \end{aligned} \tag{16}$$

Eq. (16) enables us to predict the fracture toughness from E/H, which can be directly obtained from the Vickers indentation test. It should be noted that we basically assume elastic-perfectly plastic materials in FE simulation. Hence, the yield strain

Table 6
The comparison of the fracture toughnesses obtained by Eq. (9) to those given in Anstis et al. [1] for Vickers indentation.

Material	H [a]	σ_o [b]/E [a]	ν [c]	$P_{max}/c^{3/2}$ [a,c]	K_c (MPa m$^{1/2}$)	
					Traditional method[a]	Eq. (9)
Si_3N_4 (NC132)	18.5	10.2/300	0.24	60	4.0	3.83 (−4.2)
Glass–ceramic (C9606)	8.4	4.5/108	0.24	43	2.5	2.52 (+1.0)
Si_3N_4 (NC350)	9.6	4.5/170	0.24	31	2.0	2.47 (+24)
Aluminosilicate glass	6.6	3.6/89	0.28	19	0.91	1.09 (+20)
Soda-lime glass	5.5	3.1/70	0.24	14	0.74	0.79 (+7.3)

[a] Anstis et al. [1] ($P_{max}/c^{3/2}$ values are estimated from the corresponding figure in the paper).
[b] The values obtained by trial and error method using FE analysis in the present work.
[c] Lee et al. [15].

Table 7
The comparison of fracture toughnesses obtained by Eq. (14) to a reference value for three-sided pyramidal indentation.

Indentation cracking test, Si (100), K_c = 0.7 MPa m$^{1/2}$						
ψ (°)	P_{max} (mN)	c (μm)	c/a	κ_3	Computed K_c (MPa m$^{1/2}$)	Error (%)
35.3	50	4.83	2.8	0.1495	0.704	0.6
45		4.23	2.4	0.1188	0.683	−2.4
55		3.37	1.9	0.0937	0.757	8.1
65.3		2.48	1.4	0.7078	0.906	29.5

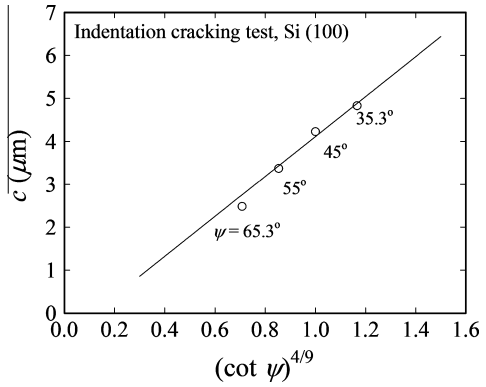

Fig. 9. The variation of c with respect to centerline-to-face angle ψ.

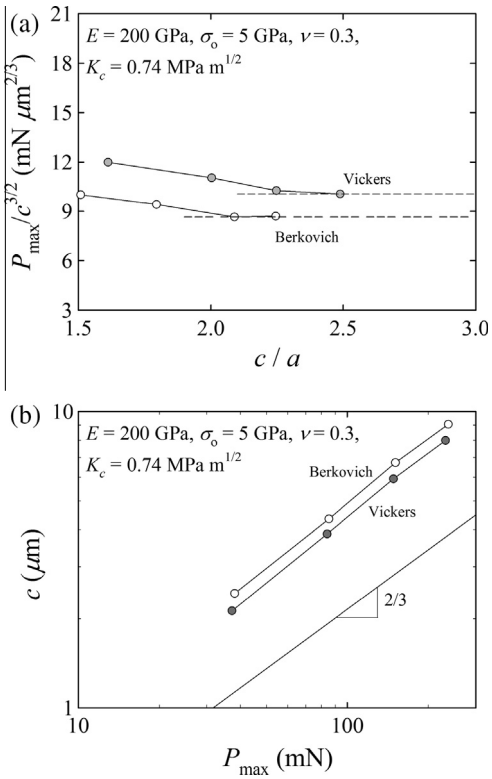

Fig. 10. (a) $P_{max}/c^{3/2}$ vs. c/a and (b) c vs. P_{max} for Vickers and Berkovich indentation.

calculated from Eq. (16) is an apparent yield strain converted from the hardness value, so the actual yield strain is always smaller than that calculated from Eq. (16). The usage of Eq. (16) is discussed in Section 4.

Table 8
The comparison of fracture toughnesses obtained from the combination of Eqs. (9) and (16) to those given in Anstis et al. [1] for Vickers indentation.

Material	$P_{max}/c^{3/2}$[a]	E/H[a]	ε_o[b]	ν[c]	K_c (MPa m$^{1/2}$)		
					Traditional method[a]	Eq. (9)	Eq. (4)
Si_3N_4 (NC132)	60	16.2	0.036	0.24	4	3.67 (−8.2)	3.87 (−3.4)
SiC	50	18.2	0.032	0.14	4	3.69 (−7.8)	3.41 (−15)
Al_2O_3 (AD999)	34	20.2	0.025	0.22	3.9	2.68 (−31)	2.44 (−37)
Al_2O_3 (AD90)	30	29.8	0.0075	0.22	2.9	3.57 (+23)	2.62 (−9.7)
Glass ceramic	43	12.8	0.053	0.24	2.5	2.05 (−18)	2.47 (−1.3)
Si_3N_4 (NC350)	31	17.7	0.031	0.24	2	2.24 (+12)	2.09 (+4.4)
Sapphire	21	19.5	0.026	0.22	2.1	1.58 (−25)	1.48 (−29)
Aluminosilicate glass	19	13.5	0.047	0.28	0.91	0.96 (+5.4)	1.12 (+23)
Soda-lime glass	14	12.7	0.054	0.24	0.74	0.67 (−9.3)	0.80 (+8.0)
Lead alkali glass	14	13.3	0.050	0.24	0.68	0.72 (+5.2)	0.82 (+20)
Si	12	15.8	0.038	0.22	0.7	0.76 (+8.9)	0.76 (+9.2)

[a] Anstis et al. [1] ($P_{max}/c^{3/2}$ values are estimated from the corresponding figure in the paper).
[b] The values obtained by Eq. (16) in the present work.
[c] Lee et al. [15].

4. Evaluation of the new formulas by using indentation test data

We compare the suggested equations to the experimental data of Anstis et al. [1] and our nanoindentation data. We first investigate the usage of Eq. (9) by comparison of Anstis et al. Vickers indentation results for brittle materials. In their Vickers indentation cracking tests, the fracture toughnesses are determined from the maximum indentation load, the crack lengths, the Young's modulus, and the hardness. However, to use Eq. (9), the yield strain and Poisson's ratio should be known values. We therefore guess the apparent yield strength (and the yield strain) that gives the hardness H from Vickers indentation FE analysis, and choose the Poisson's ratios which Lee et al. [15] have used as listed in Table 6. Anstis et al. tested fifteen materials, but it is tedious work to determine the yield strength by a trial and error method using FE analysis, so we choose only five materials and compare the results. The fracture toughnesses of the five materials that Anstis et al. [1] tested [Si_3N_4 (NC132), Glass–ceramic (C9606), Si_3N_4 (NC350), Aluminosilicate glass, Soda-lime glass] are in the range 0.74–4.0 MPa $\mu m^{1/2}$, and the H/E ratios lies between 0.6 and 0.8. The average and standard deviations between the fracture toughnesses obtained from traditional methods and Eq. (9) are about 9.5% and 11.9%, respectively. Except for Si_3N_4 (NC350), Eq. (9) yields relatively accurate fracture toughnesses. The error in fracture toughness may stem from errors in measurement of Poisson's ratio, Young's modulus and from the conventionally obtained fracture toughness itself as well as from the measured crack length.

We investigate then the effectiveness of Eq. (14) for three-sided pyramidal indenters extended from the Vickers indentation formula. Based on the nanoindentation test data on (100) Si ($K_c|_{conventional}$ = 0.7 MPa m$^{1/2}$) using three-sided indenters with various indenter angles, we predict the fracture toughness. The Nanoindenter XP (Agilent Technologies) is employed for the nanoindentnation tests. Indenter angles are ψ = 35.3° (cube-corner), 45°, 55°, 65.3° (Berkovich). The crack lengths are measured after indentation with P_{max} = 50 mN and subsequent load release. Total nine indentation tests are conducted for each indenter angle with loading rate $\dot{v}_l$ = 0.5 mN/s. The measured c and a, and fracture toughness values obtained by Eq. (14) are listed in Table 7. Material properties are taken from the values obtained by Hyun et al. [7] using the Oliver–Pharr method [18] and a trial-and-error method. (E = 138 GPa, σ_o = 5.4 GPa, and ν = 0.22) Except for the fracture toughness calculated with ψ = 65.3°, the deviation does not exceed 10% for other indenters. As shown in Table 7, the c/a ratio decreases with increasing indenter angle, and the ratio for ψ = 65.3° is 1.4 which is much smaller than 2.5. Hence, in the indentation tests with ψ = 65.3° when P_{max} = 50 mN, the cracks would not be well-developed, so that the correlation of $c \propto (\cot\psi)^{4/9}$ could not be established in Fig. 9. For this reason, the prediction error becomes greater as the indenter angle increases. Jang and Pharr [8] have mentioned that even though the c/a ratio is much smaller than that required to be "well-developed" ($c/a \ll 2.5$), the proportionality between P and $c^{3/2}$ is maintained and the fracture toughness can be therefore estimated. However, Lee et al. [15] and Hyun et al. [7] have analyzed the critical c/a ratio where the maximum indentation load P_{max} is proportional to $c^{3/2}$ as shown in Fig. 10(a), and have found that the estimated fracture toughness significantly depends on the c/a ratio if the crack is not well-developed. This discrepancy between Jang and Pharr's and our results is caused by the difference of the plotting method. Whereas linear scales are used on both the horizontal and vertical axes in Fig. 10(a), log-log scales are used in Fig. 10(b). In the log-log plot, the dependency on the c/a ratio seems to be negligible although the deviation of the $P_{max}/c^{3/2}$ in Fig. 10(a) is about 20%. Hence, to achieve accurate fracture toughness values, it is necessary to use saturated data in the linear plot. For Si, the c/a ratio and the maximum load should be greater than 2 and 150–200 mN, respectively. Consequently, for well-developed cracks only, Eq. (14) can be applied to the calculation of the fracture toughness from indentation tests for various pyramidal indenter angles and edge numbers.

In Eqs. (15) and (16), we have suggested another method to estimate the yield strain from the hardness value, which can make the suggested method more practical. To verify the usefulness of the suggested method, we calculate the fracture toughnesses from Anstis et al. [1] experimental data. The used values of $P_{max}/c^{3/2}$, E/H, ν, K_c and the apparent yield strains and fracture

Table A.1
Coefficients of Eq. (9).

	$k=0$	$k=1$	$k=2$
i = 0			
$j=0$	2.093e−1	−2.119e−1	−2.500e−3
$j=1$	−4.829e+0	3.939e+0	3.525e+0
$j=2$	5.412e+1	−5.001e+1	−5.050e+1
$j=3$	−2.243e+2	2.278e+2	2.342e+2
i = 1			
$j=0$	−1.332e−01	3.993e−01	−3.425e−01
$j=1$	4.647e+00	−1.568e+01	3.740e+00
$j=2$	−6.397e+01	1.963e+02	6.472e+01
$j=3$	2.860e+02	−7.237e+02	−8.320e+02
i = 2			
$j=0$	1.768e−01	−9.491e−01	1.195e+00
$j=1$	−8.048e+00	4.249e+01	−4.250e+01
$j=2$	1.175e+02	−5.650e+02	4.388e+02
$j=3$	−5.358e+02	2.303e+03	−1.204e+03

Table A.2
Coefficients of Eq. (15).

	$j=0$	$j=1$	$j=2$
$i=0$	9.990e+0	−5.538e+0	2.325e+0
$i=1$	3.030e+1	−1.532e+1	9.000e+0
$i=2$	3.767e+1	−1.877e+1	5.075e+1

toughnesses predicted by the combination of Eqs. (16) and (9) are listed in Table 8. The average and standard deviations of suggested method are 4% and 16.6% whereas the values of the LEM method are 2.9% and 18.9%. The deviation may stem from the estimated yield strain obtained by Eq. (16) because the effect of the material hardening is neglected. The errors can also be caused by the other data, such as the Poisson's ratio, the Young's modulus, the hardness, the fracture toughness, and $P_{max}/c^{3/2}$. However, it should be noted that the standard deviation of our method is smaller than that of the LEM method, even though our prefactor κ is purely obtained from FEA whereas the LEM prefactor α is an average value of their experimental results. Consequently, considering the errors of other material properties including fracture toughness measured by conventional methods, Eqs. (9) and (16) are very accurate and useful equations to estimate the fracture toughnesses.

The unified Eq. (14) that can be applied to all kinds of pyramidal indenters is defined by only material properties and indenter geometries. Eqs. (15) and (16), however, are valid for Vickers indentation only because the material hardness is not a material property. It is varied with the indenter angle and the number of indenter edges, so it is therefore required to individually set up the form to replace ε_o by E/H for other types of pyramidal indenters.

5. Concluding remarks

In this study, we presented indentation fracture toughness evaluation methods based on FE analysis using the cohesive zone model. We studied the influence of material properties and indenter geometries on the crack length, and set up indentation variables. We suggested some kinds of formulas to estimate the fracture toughness. The fracture toughnesses were then estimated from the indentation test data, and compared to conventional values. We drew the following conclusions:

(i) The crack size is influenced by yield strain ε_o, Poisson's ratio ν, and Young's modulus E; ε_o, ν, E_R ($\equiv E/E_{1000}$) were chosen as main parameters, and fracture toughness formulas were established. In experimental data yield strain ε_o is unknown, so ε_o was determined by comparison of material hardness. The average and standard deviations between the fracture toughnesses obtained from traditional testing methods and Eq. (9) is about 10% and 12%, respectively.

(ii) Using the relation between the number of cracks and the crack size for the equivalent indenter that gives the same ideal contact area as well as the relation between the indenter angle and the crack size for the indenters having the same number of indenter edges, the suggested fracture toughness evaluation methods for Vickers indentation can be extended to any kinds of pyramidal indenters. The unified form Eq. (14) is very accurate for well-developed cracks.

(iii) Eqs. (9) and (14) require ε_o as an input value. However, it is difficult to determine ε_o for brittle materials, and it means additional experimental data is needed. We therefore proposed a method to derive ε_o from E/H and ν. By combination of Eqs. (9) and (16) and Anstis et al.'s Vickers indentation test data, we evaluated and compared the fracture toughnesses; the average and standard deviation is approximately 4% and 17%, respectively. Hence, without experimental calibration of the prefactor κ, we can accurately evaluate the fracture toughness of brittle materials.

(iv) In this study, we simply assumed isotropic elastic-perfectly plastic materials. The material hardening and anisotropy would affect the fracture behavior, so they would be our future work.

Acknowledgements

This research was supported by Basic Science Research Program through the National Research Foundation of South Korea (NRF) funded by the Ministry of Science, ICT & Future Planning (No. NRF-2012 R1A2A2A 01046480).

Appendix A

The coefficient values of regression functions of Eqs. (9) and (15) (see Tables A.1 and A.2).

References

[1] Anstis GR, Chantikul P, Lawn BR, Marshall DB. A critical evaluation of indentation techniques for measuring fracture toughness: I, Direct crack measurements. J Am Ceram Soc 1981;64:533–8.
[2] Chiang SS, Marshall DB, Evans AG. The response of solids to elastic/plastic indentation. I. stresses and residual stresses. J Appl Phys 1982;53:298–311.
[3] Chiang SS, Marshall DB, Evans AG. The response of solids to elastic/plastic indentation. II. Fracture initiation. J Appl Phys 1982;53:312–7.
[4] Cook RF, Pharr GM. Direct observation and analysis of indentation cracking in glasses and ceramics. J Am Ceram Soc 1990;73:787–817.
[5] Evans AG, Charles EA. Fracture toughness determinations by indentation. J Am Ceram Soc 1976;59:371–2.
[6] Hill R. The mathematical theory of plasticity. Oxford, UK: Oxford University Press; 1950.
[7] Hyun HC, Rickhey F, Lee JH, Hahn J, Lee H. Characteristics of indentation cracking using cohesive zone finite element techniques for pyramidal indenters. Int J Solids Struct 2014;51:4327–35.
[8] Jang JI, Pharr GM. Influence of indenter angle on cracking in Si and Ge during nanoindentation. Acta Mater 2008;56:4458–69.
[9] Johanns KE, Lee JH, Gao YF, Pharr GM. An evaluation of the advantages and limitations in simulating indentation cracking with cohesive zone finite elements. Modell Simul Mater Sci Engng 2014;22:1–21.
[10] Laugier MT. The elastic/plastic indentation of ceramics. J Mater Sci Lett 1985;4:1539–41.
[11] Lawn BR. Fracture of Brittle Solids. 2nd ed. New York, USA: Cambridge University Press; 1993.
[12] Lawn BR, Wilshaw TR. Indentation fracture: principles and applications. J Mater Sci 1975;10:1049–81.
[13] Lawn BR, Evans AG. A model for crack initiation in elastic/plastic indentation fields. J Mater Sci 1977;12:2195–9.
[14] Lawn BR, Evans AG, Marshall DB. Elastic/plastic indentation damage in ceramics: the median/radial crack system. J Am Ceram Soc 1980;63:574–81.
[15] Lee JH, Gao YF, Johanns KE, Pharr GM. Cohesive interface simulations of indentation cracking as a fracture toughness measurement method for brittle materials. Acta Mater 2012;60:5448–67.
[16] Niihara K, Morena R, Hasselman DPH. Evaluation of K_{IC} of brittle solids by the indentation method with low crack-to-indent ratios. J Mater Sci Lett 1982;1:13–6.
[17] Niihara K. A fracture mechanics analysis of indentation-induced Palmqvist cracks in ceramics. J Mater Sci Lett 1983;2:221–3.
[18] Oliver WC, Pharr GM. An improved technique for determining hardness and elastic modulus using load and displacement sensing indentation experiments. J Mater Res 1992;7:1564–83.
[19] Ouchterlony F. Stress intensity factors for the expansion loaded star crack. Engng Fract Mech 1976;8:447–8.
[20] Palmqvist S. Method of determining the toughness of brittle materials, particularly hardmetals. Jernkontorets Ann 1957;141:300–7.
[21] Pharr GM. Measurement of mechanical properties by ultra-low load indentation. Mater Sci Engng A – Struct 1998;253:151–9.
[22] Ponton CB, Rawlings RD. Vickers indentation fracture toughness test: Part 1. Review of literature and formulation of standardised indentation equations. Mater Sci Technol 1989;5:865–72.
[23] Ponton CB, Rawlings RD. Vickers indentation fracture toughness test: Part 2. Application and critical evaluation of standardised indentation toughness equations. Mater Sci Technol 1989;5:961–76.
[24] Tanaka K. Elastic/plastic indentation hardness and indentation fracture toughness: the inclusion core model. J Mater Sci 1987;22:1501–8.
[25] Tang Y, Yonezu A, Ogasawara N, Chiba N, Chen X. On radial crack and half-penny crack induced by Vickers indentation. Proc Roy Soc A – Math Phys 2008;464:2967–84.
[26] Xia SM, Gao YF, Bower AF, Lev LC, Cheng YT. Delamination mechanism maps for a strong elastic coating on an elastic-plastic substrate subjected to contact loading. Int J Solids Struct 2007;44:3685–99.
[27] Zhang W, Subhash G. Finite element analysis of interactiong Vickers indentations on brittle materials. Acta Mater 2001;49:2961–74.
[28] Zheng LL, Gao YF, Lee SY, Barabash RI, Lee JH, Liaw PK. Intergranular strain evolution near fatigue crack tips in polycrystalline metals. J Mech Phys Solids 2011;59:2307–22.